High-Frequency Transformer Winding Model with Adequate Protection

Farzad Nasirpour, Amir Heidary, Mohamad Ghaffarian Niasar, Aleksandra Lekić and Marjan Popov

***Abstract*--High local electric field intensity in transformer windings originating from transient signals is one of the reasons for transformer failures. Due to the integration of renewable energy sources into the power grids and the increased number of transients, the likelihood of transformer catastrophic failure increases accordingly. Therefore, to ensure the reliable performance of transformers and associated power networks studying their behavior during these events is required. Accordingly, there is a need for accurate modeling of transformer windings capable of simulating electromagnetic transients. Using these models, it is possible to identify frequencies that can be dangerous to the transformer windings and to study different protection schemes. This paper aims to find an accurate analytical model of transformer winding validated by experimental measurements and to study the performance of the R-L protection device during the transient phenomena. The protection device is designed based on the winding model to introduce an impedance comparable to that of the transformer winding at critical frequencies where voltage amplification in the winding is significant. This approach ensures enhanced protection against potential transformer damage to the transformer. By using this protection scheme, the high inter-turn voltage originating from transient signals may be mitigated. At the same time, it does not affect the grid's performance during normal conditions.**

***Keywords*: High-frequency transformer model, Protection, Transformer, Transient signals.**

I. Introduction

TRANSFORMERS are among the most essential and critical components in electrical power systems [1]. Any failure in them may result in long interruptions, costly repairs, and replacement, as well as severe injuries [2,3]. Being in nonstop service in decades, and exposed to different operating conditions, transformers face enormous risks during their lifetime. Obtaining data regarding the transformer insulation system, and its internal behavior is essential for the system operators. Furthermore, one of the main requirements of smart grids is high system reliability. In this regard, it is necessary to ensure the safe and reliable performance of power transformers, using different protective schemes following the phenomena taking place in the present power system [4]. The main reason for the deterioration of transformer lifetime and possible failures is their vulnerability to fast and very fast transients in the system [5]. During these events, high-frequency overvoltages may occur at the transformer terminals, which may excite internal and external resonances in the power system. In such a case, the voltage at different points of the transformer winding can be several orders of magnitude higher than that at the transformer terminals [6], which can adversely affect the transformer insulation and may lead to failure. In the last decade, several solutions to suppress fast transients and protect transformers against resonances have been proposed [7-10]. The most common method is to use a surge arrester [10]. However, other solutions are to connect the series R-L component as a composite wire to the transformer or to utilize a parallel R-L component in series with the transformer. More about these solutions can be found in [7-9].

The present study aims to evaluate the effectiveness of a protection scheme against transient events while gaining insight into transformer behavior. To accomplish this, the authors develop a detailed transformer winding model for a broad frequency range, enabling the identification of resonance and anti-resonance frequencies, as well as voltage amplification in the winding. Subsequently by using this model, safety criteria for the winding are established. Additionally, the R-L protection device parameters are adjusted, and its effects in suppressing resonance overvoltage are studied.

The rest of the paper is organized as follows. Sections II and III deal with the high-frequency modeling of a high-voltage transformer winding. In Section IV, the critical resonance point is identified mathematically and experimentally. Section V reports on the effects of a parallel R-L circuit and explains the performed experimental test setup. Finally, the last section elaborates on the performed results and meaningful conclusions.

II. High-Frequency Model of Transformer Winding

In general, transformer models are classified as a black box-, white box-, and grey box models [11]. Black box models represent the behavior of transformers at their terminals and are used in case the interaction of the transformer with other parts of the grid is of concern. These models do not provide any or more detailed information concerning the resonance phenomena occurring in them [12].

White box models can be built based on the basic circuit elements, the values of which are dependent only on transformer geometry and materials used for transformer production. Using these models, it is possible to obtain voltage

This research work has been financially supported by the Dutch Scientific Council NWO-TTW in collaboration with TSO TenneT, DSO Alliander/Qirion, Royal Smit Transformers, and TSO National Grid, UK, under the project "Protection of Future Power System Components (PRoteuS)", no. 18699.

The authors are with the Delft University of Technology, Faculty of EEMCS, Mekelweg 4, 2628CD Delft, The Netherlands; email: {f.nasirpour, A.Heidary, M.Ghaffarianniasar, A.Lekic, M.Popov}@tudelft.nl.

Paper submitted to the International Conference on Power Systems Transients (IPST2023) in Thessaloniki, Greece, June 12-15, 2023.

and current values at different nodes, and as such, they are suitable for transient studies.

The gray box modeling approach is a trade-off between white and black box modeling schemes. This means that gray box models may also enable us to study transient phenomena in transformer winding with sufficient details. However, unlike white box models, model parameters are obtained based on measurement [13]. In this paper, the white box modeling approach is selected, and to apply this method, it is required to divide the windings into smaller parts called winding sections. Then, it is possible to model each section using circuit elements. Fig. 1 shows such a model. In this figure, $R_{conductor}$ and L_i are the resistance and inductance of section i; M_{in} shows the mutual inductance between sections i and n, C_h and $R_{dielectric}$ represent the capacitance associated with this section and its equivalent parallel resistance, and finally C_{hg} and R_{hg} are the capacitance to ground and its equivalent resistance. The studied test winding shown in Fig. 2 represents part of a winding typically used for the rated voltage of 345 kV (BIL = 1050 kV), the associated parameters are presented in Table I. To improve the voltage distribution during transients, some disks have wound-in shields, which are pointed out in Fig. 2 by red and blue blocks. Each set of shields is connected together at one point. The interconnection of the turns is represented in Figure 2, where the arrows indicate how the turns are linked to each other. In further analysis, each disk is represented by one section, as shown in Fig. 1. The procedure for computing the parameters is explained here.

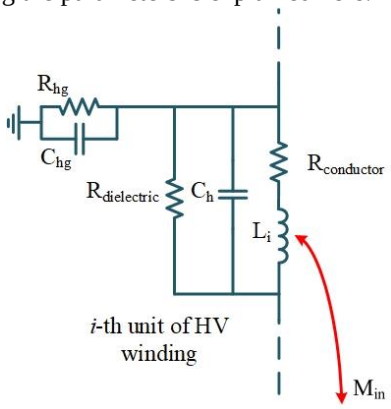

Fig. 1. Detailed model of a transformer winding.

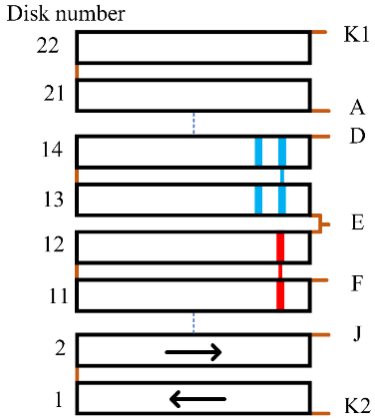

Fig. 2. The test winding used in this study. Red and blue blocks show the wound-in shields.

TABLE I
DETAILS OF THE TEST WINDING.

Number of Disks	22
Number of turns per disk	40
Conductor dimensions	1.8 mm × 8 mm
Conductor insulated dimensions	3.11 mm × 9.31 mm
Radial build	125.5 mm
Inner diameter	750 mm
Outer diameter	1001 mm
Vertical distance between disks	4 mm
Number of disks with 3 turns of shields	4
Number of disks with 2 turns of shields	4
Number of disks with 1 turns of shields	4
Number of disks with no shields	10

A. Inductances

The mutual inductance between the coils illustrated in Fig. 3 can be obtained by solving the Maxwell's equations or by applying vector potential method [14]. The expression used for the computation of the mutual inductances is [14]:

$$M_{12} = \frac{2\mu_0\sqrt{r_1 r_2}}{\sqrt{k'}}[K(k') - E(k')] \quad (1)$$

where

$$k' = \frac{1-\sqrt{1-k^2}}{1+\sqrt{1-k^2}} \quad (2)$$

$$k = \sqrt{\frac{4r_1 r_2}{(r_1+r_2)^2 + d^2}} \quad (3)$$

Here r_1 and r_2 are the mean radii of the turns, μ_0 is the permittivity of vacuum, d defines the vertical distance between turns, and K and E are the elliptical integrals of the first and second kind, respectively.

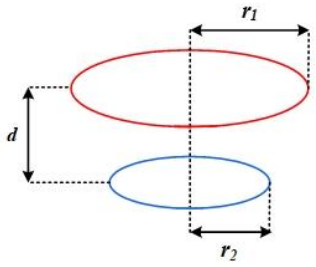

Fig. 3. The geometry of two parallel coils.

The self-inductance of the undeformed turn shown in Fig. 4 can be calculated as the mutual inductance between two identical turns having a vertical distance that is equal to the geometrical mean distance (GMD) defined as:

$$GMD = 0.2235(a+b) \quad (4)$$

where a and b are the width and the height of the coil, as shown in Fig. 4. To verify the accuracy of the method, the values obtained by the finite element method (FEM), and the analytical formula are compared. For this purpose, COMSOL Multiphysics and magnetic field (mf) module are used. Fig. 5 compares the self-inductance of disk number 1, and the mutual inductances between this disk and others obtained using analytical formula and FEM.

B. Capacitances

The capacitance associated with each disk can be calculated by applying the energy method. Fig. 6 shows an illustration of a high-voltage disk without wound-in shields with the equipot-

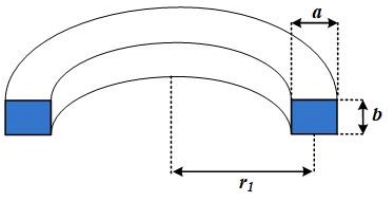

Fig. 4. The geometry of an un-deformed turn.

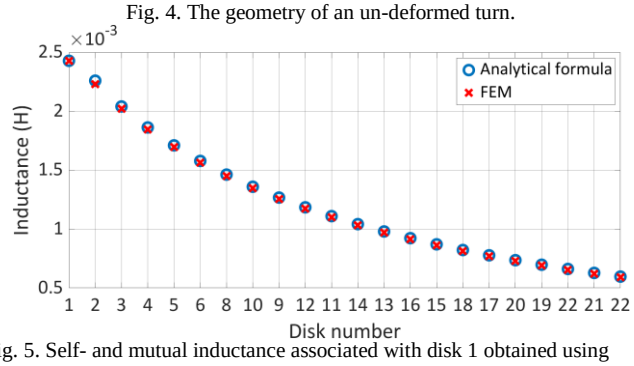

Fig. 5. Self- and mutual inductance associated with disk 1 obtained using FEM and analytical formula. At 1 is the self-inductance of this disk, and others are the mutual inductance between different disks and disk 1.

-ential surfaces between disks. The capacitance associated with this disk can be obtained using the Stein expression [15]:

$$C_h = C_s\{\frac{1}{2}\frac{\alpha}{\tanh(\alpha)} + \frac{1}{2}\frac{\alpha}{\sinh(\alpha)} + \frac{\alpha^2}{4}\} \quad (5)$$

$$C_s = \frac{C_{tt}(N_t - 1)}{{N_t}^2} \quad (6)$$

$$\alpha = \sqrt{\frac{4C_{dd}}{C_s}} \quad (7)$$

In (5) to (7), C_{tt} and C_{dd} are the capacitance between the two adjacent turns in a disk, and the total capacitance between two adjacent disks, respectively, whilst N_t is the number of turns in each disk. C_{tt} and C_{dd} can be obtained by (8) and (9):

$$C_{tt} = \frac{\varepsilon_0\varepsilon_p 2\pi R_{ave}(h + 2\tau_p)}{\tau_p} \quad (8)$$

$$C_{dd} = \frac{\varepsilon_0\pi({R_{out}}^2 - {R_{in}}^2)}{(\frac{\tau_p}{\varepsilon_p} + \tau_a)} \quad (9)$$

in which R_{ave}, R_{out}, and R_{in} are the mean, outer, and inner radius of the disks, respectively. h is the height of the conductor without insulation, ε_p and ε_0 represent paper relative permittivity and the permittivity of vacuum, respectively. τ_p is the double one-sided insulation of the conductor, and τ_a is the distance between disks.

The capacitance of a pair disk with wound-in shields is obtained by [16]. The approach can be modified to obtain the capacitance of each wound-in shield disk, as shown in Fig. 7, with respect to equipotential lines. The total electrostatic energy stored between these equipotential lines can be written as (10):

$$E_{tot} = E_{tot_{tt}} + E_{tot_{ts}} + E_{tot_{dd}} \quad (10)$$

in which $E_{tot_{tt}}$, $E_{tot_{ts}}$, and $E_{tot_{dd}}$ are the total energy stored between turns, between turns and shields, and between disks, respectively. Assuming a linear voltage distribution in the winding, $E_{tot_{dd}}$ may be obtained as:

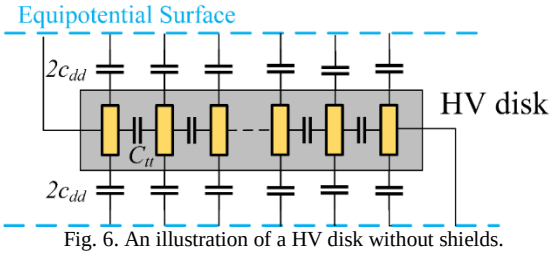

Fig. 6. An illustration of a HV disk without shields.

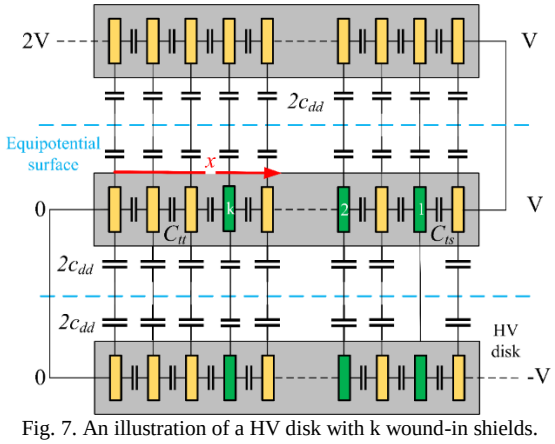

Fig. 7. An illustration of a HV disk with k wound-in shields.

$$E_{tot_{dd}} = \frac{1}{2}(2c_{dd})\int_0^L [\left(\frac{V}{L}x\right)^2 + \left(\frac{V}{L}x - V\right)^2]dx = \frac{1}{2}\left(\frac{4}{3}c_{dd}L\right)V^2 \quad (11)$$

being L the total length of the disk, V the voltage drop on it, and c_{dd} the capacitance between turns of adjacent disks, as shown in Fig. 7. $E_{tot_{tt}}$ can be obtained using (12):

$$E_{tot_{tt}} = \frac{1}{2}(\frac{N_t - k - 1}{N_t^2}C_{tt})V^2 \quad (12)$$

in which, k is the number of wound-in shields in each disk. Finally, the energy stored between shield number i and its adjacent turns can be obtained using:

$$E_{ts} = \frac{1}{2}C_{ts}[\frac{V^2}{N_t^2}(N_t^2 + (N_t - 1)^2)\,] \quad (13)$$

Equation (13) was obtained assuming that the potential of the wound-in shields also changes linearly, and the outer-most shields are at zero potential. Since in total there are k shields in the disk, $E_{tot_{ts}}$ can be expressed according to (14):

$$E_{tot_{ts}} = \frac{1}{2}[C_{ts}\frac{k(N_t^2 + (N_t - 1)^2)}{N_t^2}]V^2 \quad (14)$$

The total capacitance of the wound-in shield disk can now be obtained using (15) having in mind that $C_{dd} = c_{dd}L$.

$$C_h = \frac{4}{3}C_{dd} + \frac{N_t - k - 1}{{N_t}^2}C_{tt} + C_{ts}[\frac{k(N_t^2 + (N_t - 1)^2)}{N_t^2}] \quad (15)$$

In (15), C_{ts} is the capacitance between the turns and the shields and it can be obtained by (8). There are some uncertainties regarding the value of the relative permittivity of the insulation paper. For oil-impregnated insulation paper, it is in the range of 3 to 4. However, the paper used in the test winding is dry, and this implies that a large part of it, is filled

with air resulting in a lower combined permittivity. As it was not possible to measure the actual permittivity of the paper, different values have been considered. The value of 1.4 for the relative permittivity of the paper shows the best fit with the experimental results and is used in this paper. According to [15], the relative permittivity of 1.5 for the paper in air corresponds to the effective density of 0.5 g/cm^3, which may result in relative permittivity of 3 for the same paper in oil. This shows that assuming the value of 1.4 for the relative permittivity of the paper is realistic.

A. Resistances

The value of the resistances which are used in the model represents the conductor's resistances and the losses in the insulation. Due to the skin and proximity effects, the computation of the AC resistance of the conductors is very sophisticated, as it involves finding magnetic flux in the conductors in a complex geometry. Hence, only the DC resistance of the conductors is considered here.

The relation between the dissipation factor and the frequency for oil-impregnated paper is obtained by [17], and is as:

$$\tan\delta = 1.082\times10^{-8}\omega + 5\times10^{-3} \quad (16)$$

Although the paper, in this case, is not impregnated with oil, yet, expression (16) can be used as a rough estimation for the dissipation factor, as the behavior of the paper in both cases should not change drastically. As mentioned before, due to the high moisture level in the test case, it shows a higher level of power loss in its dielectric. To include this effect in the model, expression (16) has been modified as:

$$\tan\delta = 1.082\times10^{-8}\omega + 70\times10^{-3} \quad (17)$$

Considering the dissipation factor, the equivalent resistance that represents the dielectric losses can be obtained using (18):

$$R_{dielectric} = \frac{1}{\tan\delta\, C_h\omega} \quad (18)$$

in which C_h is the capacitance computed before, and ω is the angular frequency.

III. Transformer Admittance Matrix

Having the values of the elements, it is easy to construct the admittance matrix of the transformer winding. Firstly, the capacitance, resistance, and inductance matrices are obtained, and thereafter the admittance matrix is constructed. The procedure to construct these matrices is explained here below.

A. Capacitance and dielectric resistance matrices

The capacitance matrix is a nodal matrix. As the studied case has 22 disks, and each disk is considered as one section, there are 23 nodes in total. The diagonal element of the matrix, C_{ii}, is the sum of all the capacitances connected to node i. The non-diagonal element C_{ij} is the capacitance between node i and j with the negative sign. The same procedure should be followed for the dielectric resistance matrix.

B. Inductance and conductor resistance matrices

The inductance matrix is a branch matrix. Considering the number of the sections, the size of the inductance matrix would be 22 by 22. The diagonal element of this matrix, L_{ii}, is the self-inductance of section i, and the non-diagonal element L_{ij} is the mutual inductance between section i and j.

The conductor resistance matrix should also be constructed on the same basis, except that mutual resistances are ignored in this study, and hence non-diagonal elements would be zero.

C. Admittance matrix

The admittance matrix of the transformer can be obtained using (19) and (20):

$$Y = \Gamma + j\omega C + \frac{1}{R_d} \quad (19)$$

$$\Gamma = k(R_c + j\omega L)^{-1}k^T \quad (20)$$

in which C, L, R_d, R_c, and k are the capacitance, inductance, dielectric resistance, conductor resistance, as well as incidence matrices, respectively, and T denotes matrix transposition. By inverting the admittance matrix, the impedance matrix can be obtained:

$$Z = Y^{-1} \quad (21)$$

IV. Verification of The Model

The diagonal elements of the impedance matrix, Z_{ii}, is the impedance seen from node i. To validate the model, the response of the winding for different configurations is measured. This has been done by using Omicron Bode 100 device which is capable of determining the sweep frequency characteristics. Fig. 8 compares Z_{11}, the harmonic terminal impedance of the winding obtained from the analytical model and the measurement.

As can be seen, there is a good agreement between the response obtained from the model and the measurements. The difference in the high-frequency part is the result of the stray capacitances originating from the connections and the cables.

Considering (21), the voltage at node j when node i is excited can be computed according to (22) having the end-winding terminal grounded:

$$V_j = \frac{Z(i,j)}{Z(i,i)}V_i \quad (22)$$

Fig. (9) and (10) compare the voltage at nodes D and F when node K2 is excited, and node K1 is grounded with respect to node K_2. It should be noted that these results are obtained using a 50 Ω resistance for the voltage measurement, and therefore, a 50 Ω resistance is also added to the model. The same level of accuracy can be seen here as well. Thus, us-

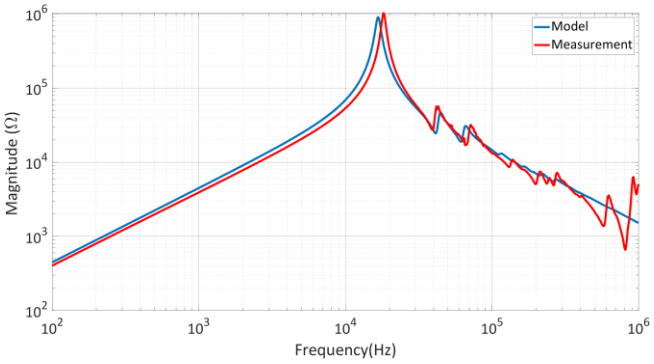

Fig. 8. Terminal impedance of the test winding.

-ing this model, the voltage distribution along the winding for a broad frequency range can be studied.

It is also important to see how the voltage is amplified in the transformer winding since it can lead to very high local electric field intensity, damaging the insulation and leading to a winding failure. Equation (22) can be used to obtain the amplification factor when one end of the winding is grounded. Fig. 11 shows the amplification factor at different nodes with respect to node K2 for the frequency range of 100 Hz up to 1 MHz obtained through a simulation model. It can be seen that at 41 kHz, the voltages of nodes E and D can be 1.8 times higher than that at the terminal. To examine this, the amplification factors for all the nodes and the same frequency range are measured. The measurement shows that at the frequency of 37.8 kHz, the same nodes have the maximum amplification factor among other nodes, which is 1.8. The difference between the resonance frequency predicted by the model and obtained by measurements is less than 10%. The amplification factors for nodes E and J are compared with the model and shown in Fig. 12.

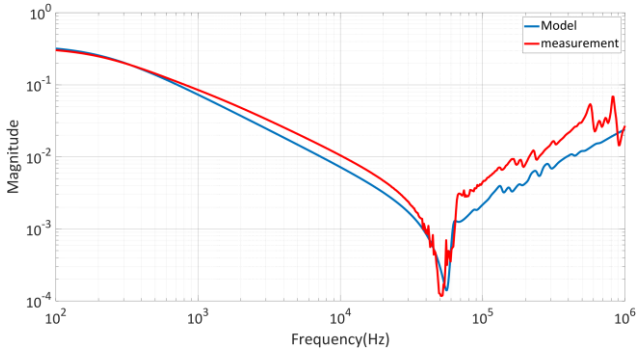

Fig. 9. The voltage at node D with respect to node K2.

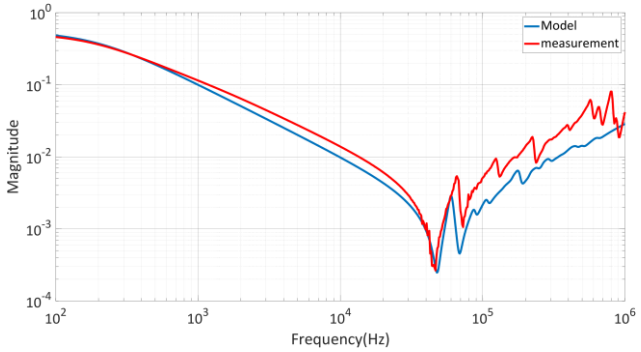

Fig. 10. The voltage at node F with respect to node K2.

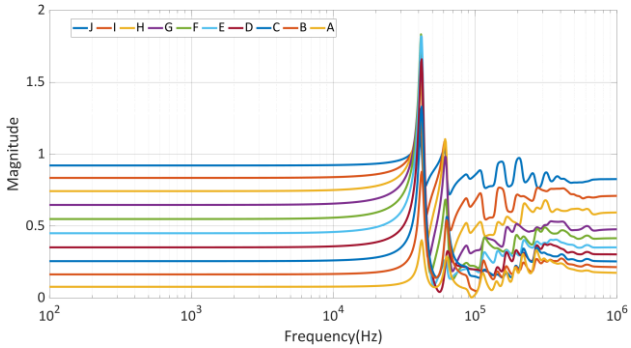

Fig. 11. The voltage at different points with respect to the node K2 obtained by model.

The differences in the high-frequency range are noticeable. This is due to the capacitances of the measurement cables and connections, which can affect the results at higher frequencies. Nevertheless, the model provides the correct answer to three essential matters:

- critical frequency ranges,
- the amplification factors at these points,
- the nodes that experience the highest voltage and local electric field.

The data provided by this model can lead to optimized protection schemes against transient phenomena, the results of which are presented in the next section.

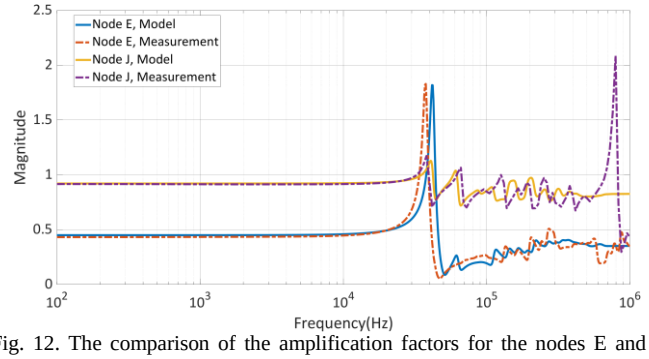

Fig. 12. The comparison of the amplification factors for the nodes E and J obtained by the measurement and by the computer model.

V. Performance Evaluation of R-L Protection Circuit

In this section, an R-L protection device against transient (PDAT) is developed to suppress the overvoltage occurring in the winding in case of resonance. When high-frequency transients occur, the voltage drop on the PDAT increases to preserve the winding from the resonance overvoltages. Using the data provided by the model of the studied winding, the parameters of the protection device can be adjusted. Here, the critical considerations for the design of PDAT are the resonance voltage of the winding besides its impedance. By applying suitable series impedance with the transformer, the voltage of the winding in the resonance point will be limited to an acceptable magnitude. This approach is illustrated in Fig. 13.

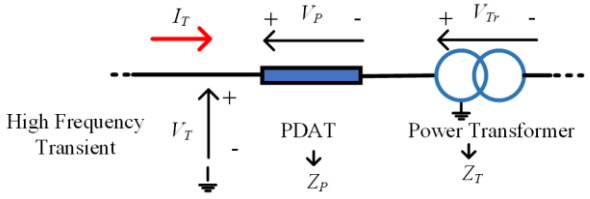

Fig. 13. Connection of PDAT with the transformer in a network segment.

By taking Fig. 13 into account, the expressed conditions in (23)-(25) are considered to design PDAT where the protection device is adjusted for the most critical frequency point obtained by the model.

$$V_{Tr} \leq V_{safe} \tag{23}$$

$$V_{Tr} = \frac{V_T . Z_T}{Z_T + Z_P} \tag{24}$$

$$\frac{V_T . Z_T}{Z_T + Z_P} \leq V_{safe} \quad (25)$$

Here, V_T is the magnitude of the frequency component of transient voltage, which results in the highest AF, V_{Tr} is the maximum amplified voltage in the transformer winding, and V_{safe} is the safe operating voltage of the transformer, considering the isolation restriction that should be achieved. Z_T and Z_P are the impedances of transformer winding and PDAT at the resonance frequency, respectively. Therefore, the impedance of PDAT in resonance frequency can be adjusted as follows:

$$\left(\frac{V_T . Z_T}{V_{safe}}\right) - Z_T \leq Z_p \quad (26)$$

Using (26), the minimum impedance which is needed to impose by PDAT can be calculated. The structure of PDAT is depicted in Fig. 14, which consists of a ferromagnetic core, placed around the transmission line, and a resistance in its secondary.

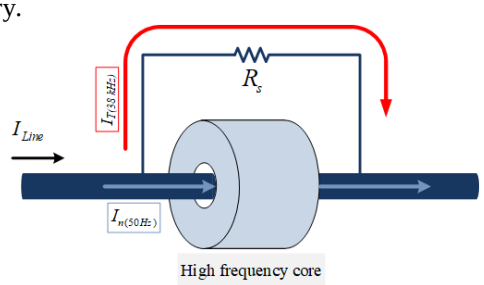

Fig. 14. Structure of PDAT.

The purpose of adding a parallel resistance R_s to the protection circuit is to conduct the high-frequency contents of transient current and dissipate the energy of the transient signal in the resistive branch. In such a case, the impedance of the inductive branch is much higher, which means it only conducts a small part of the high-frequency current. In contrast, the line current I_n is conducted through the inductive branch in the normal condition.

In the laboratory setup, V_{safe} is considered as 1 p.u. (voltage of insulation part safe operation). To simulate the higher voltage originated from transient signals, the magnitude of the high-frequency voltage source is adjusted to be 1.5 p.u.. It should be noted that this value is considered only for the sake of an explanation of the methodology. By implementing the setup as shown schematically in Fig. 15 and experimentally in Fig. 16, the voltage of transformer winding with and without connecting PDAT is examined. By applying the values of transient voltage and impedance of the transformer winding at the resonance frequency in expression (26), PDAT impedance is calculated as follows:

$$Z_{P(41kHz)} \geq 10 \times 10^3 \Omega \quad (27)$$

This impedance is designed basically using (28):

$$Z_{P(41kHz)} = \frac{R_s . Z_{in}}{R_s + Z_{in}} \geq 10 \times 10^3 \quad (28)$$

Here R_s is the parallel resistor and Z_{in} is the impedance of the inductive branch. In the first step of the test, the winding is excited by a sinusoidal signal with a frequency of 37.8 kHz, which is the measured critical frequency of the winding. Fig. 17 shows the voltage of nodes E and K2 without PDAT (considering that the bypass switch is ON). In this case, it is observable that the voltage of node E of the winding is 1.8 times higher than the voltage at the terminal and is 2.7 higher than the assumed safe voltage.

Fig. 18 shows the same signals by using PDAT, where the magnitude of node E is limited to the safe voltage of 1 p.u.. This operation proves the effective protection of the winding against transient resonance. The data of the implemented laboratory setup and measured values are presented in Table II.

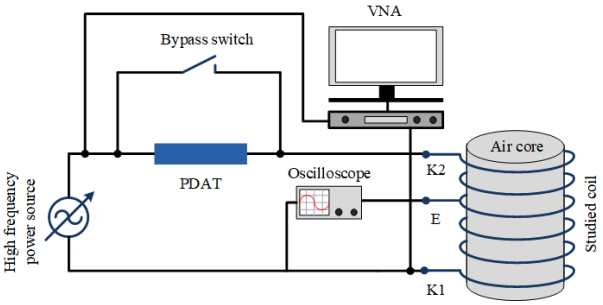

Fig. 15. Laboratory setup diagram.

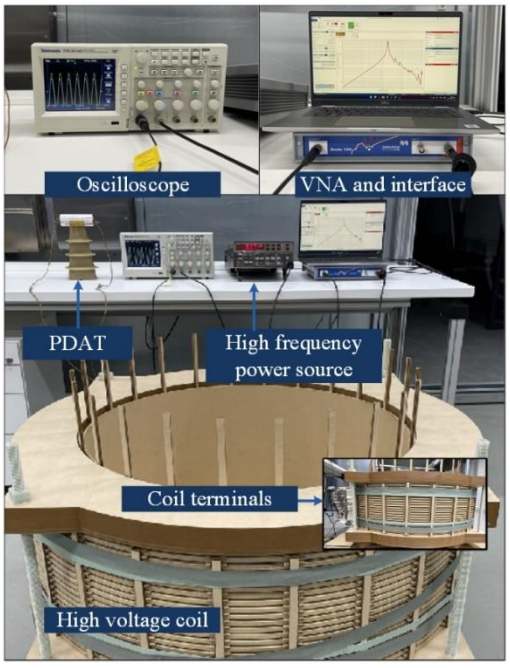

Fig. 16. Laboratory implemented setup.

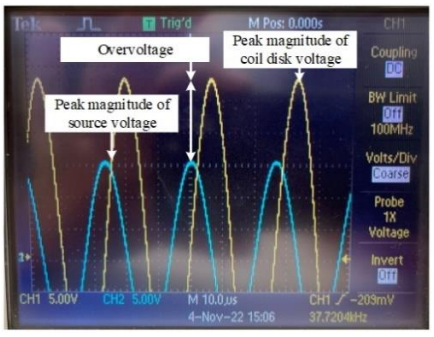

Fig. 17. The voltage at node E without protection device.

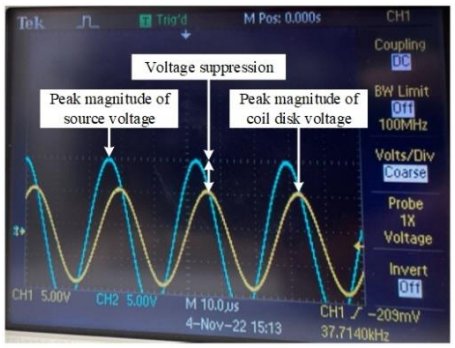

Fig. 18. The voltage at node E with protection device.

TABLE II
DETAILS OF THE LABORATORY SETUP AND MEASUREMENT

Laboratory equipment data	**Detail**
High-frequency source	50 Hz - 1 MHz, 0-25V, 50 W
Oscilloscope	Laboratory oscilloscope TDS2014B
impedance analyzer, VNA	Frequency sweep Omicron Bode100
Protection device impedance (50 Hz)	Z=100 mΩ
Protection device impedance (resonance frequency)	Z=10 kΩ
Peak voltage without protection	2.7 p.u.
Peak voltage with protection	1 p.u.

VI. CONCLUSION

In this paper, a high-frequency transformer winding model is developed that can be used to compute the voltage distribution along the winding and to find its resonance frequencies. The model was validated through experimental measurements. Furthermore, using the data provided by the model, a protection device against transient (PDAT) was developed. This scheme aims to provide an impedance close to transformer impedance in resonance frequency to suppress occurred overvoltage. The analytical studies and experimental validation confirm the proper operation of the PDAT circuit to protect the studied winding against overvoltage in resonance status.

VII. FUTURE WORK

Although using the R-L protection device shows promising results when applied to small coils and transformers, its performance regarding the large transformers needs further investigation, as it should impose much higher impedance at resonance frequencies. Besides, it must dissipate a significant amount of power. In addition, the consideration of the magnitude of voltage drop and the isolation design of the protection device can be a crucial challenge. Furthermore, transformers are normally connected to cables or lines on both high-voltage and low-voltage sides. Hence, in general, it will be important in the future to observe possible resonance frequencies of the whole system consisting of cable-transformer connection and do more research on how to design cheap protection solutions to prevent the occurrence of resonances.

VIII. ACKNOWLEDGMENT

The authors gratefully acknowledge the contributions of Royal SMIT Transformers B.V. for providing a test winding and data for this research project.

IX. REFERENCES

[1] A. Abu-Siada and S. Islam, "A novel online technique to detect power transformer winding faults," IEEE *Tran. Power Delivery*, vol. 27, no. 2, pp. 849-857, 2012.

[2] V. Nurmanova, M. Bagheri, A. Zollanvari, K. Aliakhmet, Y. Akhmetov, and G. B. Gharehpetian, "A new transformer FRA measurement technique to reach smart interpretation for inter-disk faults," *IEEE Tran. Power Delivery*, vol. 34, no. 4, pp. 1508-1519, 2019.

[3] J. Chong and A. Abu-Siada, "A novel algorithm to detect internal transformer faults," in *2011 IEEE Power and Energy Society General Meeting*, 2011: IEEE, pp. 1-5.

[4] M. Bagheri, M. S. Naderi, T. Blackburn, and T. Phung, "Practical challenges in online transformer winding deformation diagnostics," in *2011 2nd International Conference on Electric Power and Energy Conversion Systems (EPECS)*, 2011: IEEE, pp. 1-6.

[5] S. H. Hosseini, M. Vakilian, and G. B. Gharehpetian, "Comparison of transformer detailed models for fast and very fast transient studies," *IEEE Tran. Power Delivery*, vol. 23, no. 2, pp. 733-741, 2008.

[6] M. Popov, "General approach for accurate resonance analysis in transformer windings," *Electric Power Systems Research*, vol. 161, pp. 45-51, 2018.

[7] D. Smugala, W. Piasecki, G. Bywalec, M. Ostrogorska, O. Granhaug, and P. Skryten, "Very fast transient suppressing device," ed: Google Patents, 2015.

[8] W. Piasecki, G. Bywalec, M. Florkowski, M. Fulczyk, and J. Furgal, "New approach towards very fast transients suppression," in *Proceedings of IPST*, 2007.

[9] A. Heidary, K. Rouzbehi, H. Radmanesh, and J. Pou "Voltage Transformer Ferroresonance: An Inhibitor Device," *IEEE Transactions on Power Delivery*, vol. 35, no. 6, pp. 2731-2733, Dec. 2020.

[10] Y. Zhang, Q. Yang, S. Xie, and C. Zhang, "Mechanism and application of arrester block voltage division to lightning transient voltage monitoring in substation transformers," *IEEE Trans. Electromagnetic Compatibility*, vol. 61, no. 3, pp. 689-696, 2019.

[11] M. García-Gracia, M. Villén, M. Cova, and N. El Halabi, "Detailed three-phase circuit model for power transformers over wide frequency range based on design parameters," *Electric power systems research*, vol. 92, pp. 115-122, 2012.

[12] T. A. Papadopoulos, A. I. Chrysochos, A. I. Nousdilis, and G. K. Papagiannis, "Simplified measurement-based black-box modeling of distribution transformers using transfer functions," Electric Power Systems Research, vol. 121, pp. 77-88, 2015.

[13] R. Aghmasheh, V. Rashtchi, and E. Rahimpour, "Gray box modeling of power transformer windings for transient studies," *IEEE Tran. Power Delivery*, vol. 32, no. 5, pp. 2350-2359, 2017.

[14] E. Rahimpour, J. Christian, K. Feser, and H. Mohseni, "Transfer function method to diagnose axial displacement and radial deformation of transformer windings," *IEEE Tran. Power Delivery*, vol. 18, no. 2, pp. 493-505, 2003.

[15] R. M. Del Vecchio, B. Poulin, P. T. Feghali, D. M. Shah, and R. Ahuja, *Transformer design principles*. CRC press, 2017.

[16] M. G. Niasar and W. Zhao, "Impulse voltage distribution on disk winding: calculation of disk series capacitance using analytical method," in *2020 IEEE International Conference on High Voltage Engineering and Application (ICHVE)*, 2020: IEEE, pp. 1-4.

[17] E. Rahimpour, "Hochfrequente Modellierung von Transformatoren zur Berechnung der Übertragungsfunktion [High Frequency Modeling of Transformers using the Transfer Function]," *Ph. D. dissertation, University of Stuttgart*, 2001.